2014/12/02
Head Id: 269969
Archive Id: 269969P
Archive Date: 2014/12/02
Archive Tag: trunk

Search for invisible decays of Higgs bosons in the vector boson fusion production mode

The CMS Collaboration

Abstract

A search for invisible decays of Higgs bosons in the vector boson fusion (VBF) production mode is carried out using data recorded in 2012 at a centre-of-mass energy of 8 TeV by the CMS detector corresponding to an integrated luminosity of 19.2 inverse femtobarns. Limits are set on the production cross section times invisible branching fraction, as a function of the Higgs boson mass. Assuming standard model Higgs boson cross sections and acceptances, the observed (expected) upper limit on the invisible branching fraction at $m_{\mathrm{H}} = 125\,\mathrm{GeV}$ is found to be 0.XX (0.38) at 95% confidence level.

The search for invisible decays of Higgs bosons has been extensively studied in the past [1–3], and at the LHC with the full 7 and 8 TeV datasets, by both the ATLAS [4, 5] and CMS [6] collaborations. Assuming standard model (SM) Higgs boson cross sections and acceptances, the ATLAS collaboration places an upper limit on the Higgs boson invisible branching fraction, $\mathcal{B}(\mathrm{H} \to \mathrm{inv})$, of 0.75 at 95% CL for $m_{\mathrm{H}} = 125.5\,\mathrm{GeV}$, using the associated ZH production mode [4, 5]. By combining both vector boson fusion (VBF) and associated ZH production modes, the CMS collaboration is able to set an observed (expected) upper limit on $\mathcal{B}(\mathrm{H} \to \mathrm{inv})$at $m_{\mathrm{H}} = 125\,\mathrm{GeV}$ of 0.58 (0.44) at 95% confidence level. An extensive introduction to the motivations for such a search and an overview of the theoretical models proposing invisible decay channels of either SM like or heavier Higgs bosons can be found in Ref. [6].

In the analysis presented in this letter, the sensitivity of the CMS VBF analysis is improved significantly through the use of a new set of signal selection criteria made possible by different triggers with looser thresholds than the trigger used for the previous analysis. The total integrated luminosity re-analysed is $19.2 \pm 0.5\ \mathrm{fb}^{-1}$ [7].

The central feature of the CMS apparatus is a superconducting solenoid of 6 m internal diameter, providing a magnetic field of 3.8 T. Within the volume of the superconducting solenoid are a silicon pixel and strip tracker, a lead tungstate crystal electromagnetic calorimeter (ECAL), and a brass-scintillator hadron calorimeter, each composed of barrel and endcap detectors. Muons are measured with detection planes made using three technologies: drift tubes, cathode strip chambers, and resistive-plate chambers, embedded in the steel flux-return yoke outside the solenoid. Extensive forward calorimetry complements the coverage provided by the barrel and endcap detectors. Data are selected online using a two-level trigger system. The first level (L1T), consisting of custom made hardware processors, selects events in less than $1\,\mu\mathrm{s}$, while the high-level trigger (HLT) processor farm further decreases the event rate from around 100 kHz to a few hundred Hz before data storage. A more detailed description of the CMS apparatus, together with a definition of the coordinate system used and the relevant kinematic variables, can be found in Ref. [8].

In 2012, in order to make full use of the maximum storage rate available, two parallel data-taking streams were put in place. The first was the standard "prompt" data stream, which was reconstructed immediately. The second was the "parked" data stream, which was taken using looser versions of some of the "prompt" stream triggers, and was reconstructed later on in 2013 during the long shutdown of the LHC.

The analysis presented here uses the same event cleaning, object definitions and Monte Carlo (MC) samples as described in Ref [6]. The VBF signal is simulated using the POWHEG 2.0 event generator [9–15]. The VBF production cross sections are taken from Refs. [16, 17]. The main background processes, namely W, Z, and $\mathrm{t\bar{t}}$ produced in association with jets, are simulated using MADGRAPH 5.1.1 [18] interfaced with PYTHIA 6.4.26 [19]. The QCD multijet background is simulated with PYTHIA 6.4.26 [19]. Detector effects are then simulated using the GEANT4 package [20]. All MC samples are reweighted event-by-event to reproduce the distribution of minimum bias interactions (pileup) observed in data.

The signatures of an invisibly decaying VBF produced Higgs are jets and missing transverse energy, these in addition to leptons which are required by several background estimation methods, are the main objects used in this analysis. These objects are reconstructed with a particle-flow ("PF") algorithm [21, 22]. Pileup mitigation techniques are in place to correct the objects, as described in detail in Ref [6].

Electrons (muons) are selected in the pseudorapidity range $|\eta| < 2.4(2.1)$ and with $\mathrm{p}_T >$

10 GeV. For electrons, the $1.44 < |\eta| < 1.57$ transition region between the ECAL barrel and endcap is excluded. Different isolation and identification criteria are used depending on whether the lepton is explicitly required, where tighter criteria and $p_T > 20$ GeV are required, or vetoed, where looser criteria and $p_T > 10$ GeV are required. A loose isolation requirement is still applied for veto leptons, implying that leptons in jets will a priori not be removed. Hadronic taus are identified using the "hadron-plus-strips" algorithm [23] which reconstructs the main hadronic tau decay modes using charged hadrons and photons, and leads to an expected efficiency of 55% for a fake rate less than 3%, for taus with $p_T > 20$ GeV and $|\eta| < 2.3$. MC samples are reweighted event-by-event to match the lepton reconstruction, identification and isolation efficiencies measured in data.

Jets are clustered using the anti-k_T clustering algorithm [24], with a distance parameter of 0.5, as implemented in the FASTJET package [25, 26]. Jets are selected in the pseudorapidity range $|\eta| < 4.7$ and with $p_T > 30$ GeV. Jet energy corrections are applied [27], as well as identification criteria to remove contributions from calorimeter noise or from pileup interactions. Jets with a veto electron or a loose muon within $\Delta R < 0.5$ are filtered out.

We define the missing transverse energy, E_T^{miss} and $\phi_{E_T^{miss}}$ as the modulus and azimuthal angle of the negative vectorial sum of all PF objects except the muons. Muons are neglected in the calculation of the E_T^{miss} from trigger level onwards to increase the number of events in background estimation control regions where muons are required. Jet energy corrections (including effects from pileup) are propagated to the E_T^{miss} object.

The same analysis strategy as in Ref. [6] is used. The pair of jets from VBF production have the distinct topology of being well separated in η, in opposite forward/backward halves of the detector, and having a high dijet invariant mass, M_{jj}. Final states with two jets with this VBF topology and large missing transverse energy are therefore selected.

The triggers available during 2012 varied across different data-taking periods. For each period the unprescaled VBF-specific trigger with the loosest selection criteria is used, this leads to three different triggers being used in total. All three have the same L1T selection, requiring L1T $E_T^{miss} > 40$ GeV (this is calorimeter-based only, so equivalent to E_T^{miss}). The first trigger is the same as the prompt trigger used in Ref. [8], and selects, among all possible jet pairs to minimise the impact of pileup, at least one pair of PF jets with $p_T > 40$ GeV, $E_T^{miss} > 65$ GeV, $M_{jj} > 800$ GeV and dijet pseudorapidity difference $\Delta\eta_{jj} > 3.5$. The first (second) parked trigger selects a pair of calorimeter jets with $p_T > 35(30)$ GeV, $M_{jj} > 700$ GeV and $\Delta\eta_{jj} > 3.5$. To take into account the correlations between the different variables, the efficiency of each trigger is measured as a function of E_T^{miss} in bins of M_{jj} and sub-leading jet p_T, using events recorded by a single-muon trigger. All MC samples are then weighted event-by-event by the luminosity-weighted average of the three measured efficiencies.

The data recorded by the triggers is dominated by QCD multijet events. Multijet events have two very distinct origins: (1) events with fake E_T^{miss}, where the E_T^{miss} comes from mismeasured jets in the events; and (2) events with genuine E_T^{miss}, where the E_T^{miss} comes from the decay of hadrons involving neutrinos, in particular heavy-flavour decays. The fake E_T^{miss} contribution can be reduced by requiring the E_T^{miss} significance $\frac{E_T^{miss}}{\sigma(E_T^{miss})}$, defined as the ratio of the vectorial over scalar sums of the transverse energy of the reconstructed PF candidates, to be large. Both components can be reduced by isolating the E_T^{miss}, by requiring that the minimum azimuthal angle separation between any reconstructed jet with $p_T > 30$ GeV and the E_T^{miss}, $\min\Delta\phi(E_T^{miss}, j)$, be large.

The trigger requirements together with reducing the QCD multijet contribution to negligible

levels drive the choice of the following selection:

$$\begin{aligned} &\eta_{j1} \cdot \eta_{j2} < 0,\ \eta_{j1,2} < 4.7, \\ &\text{jet 1 } p_T > 50\,\text{GeV},\ \text{jet 2 } p_T > 40\,\text{GeV}, \\ &\Delta\eta_{jj} > 3.6,\ \text{GeV},\ M_{jj} > 1000\,\text{GeV}, \\ &E_{\mathrm{T}}^{\mathrm{miss}} > 90\,\text{GeV}, \\ &\min\Delta\phi(E_{\mathrm{T}}^{\mathrm{miss}}, \mathrm{j}) > 2.0,\ \frac{E_{\mathrm{T}}^{\mathrm{miss}}}{\sigma(E_{\mathrm{T}}^{\mathrm{miss}})} > 4. \end{aligned} \tag{1}$$

At this stage in the selection, the background processes leading to a similar final state are, by order of decreasing importance: the associated production of W and Z with jets, QCD multijet production, all top channels ($t\bar{t}$, single top and tW channels), dibosons, and Drell–Yan($\ell\ell$)+jets. The selection is further optimised by tightening the requirements listed above to find the best 95% C.L. expected limit on $\mathcal{B}(\mathrm{H} \to \mathrm{inv})$for a m_{H}=125 GeV Higgs boson. The optimal additional selection is found to be $\min\Delta\phi(E_{\mathrm{T}}^{\mathrm{miss}}, \mathrm{j}) > 2.3$, $\mathrm{p}_T^{j2} > 45\,\text{GeV}$ and $\mathrm{M}_{jj} > 1200\,\text{GeV}$, and these requirements along with those above are used to define the signal region.

Except for the very minor dibosons and DY contributions which are directly taken from MC, all other backgrounds are normalised to the data using independent control regions. In the case of the W, Z and top background processes, the control regions are defined by replacing the signal region's lepton veto with a requirement for either exactly one lepton (electron, muon or hadronic tau), exactly two muons, or exactly one electron and one muon, in order to enrich the sample in W, Z or top events respectively. Except in the top and W$\to \tau_{\mathrm{h}}$ control regions, where the small number of events requires further differences all other requirements in the control regions are the same as those in the signal region. In the top control region, the number of events passing the selection and the QCD multijet background is negligible, therefore the requirement on $\min\Delta\phi(E_{\mathrm{T}}^{\mathrm{miss}}, \mathrm{j})$is dropped. In the W$\to \tau_{\mathrm{h}}\nu$ control region, the criteria on $\min\Delta\phi(E_{\mathrm{T}}^{\mathrm{miss}}, \mathrm{j})$is loosened to 1, and an additional requirement that the transverse mass of the W be greater than 20 GeV is used to reject the small remaining QCD contribution. By studying the W$\to \mu\nu$ region (which has enough events to observe the full range of the $\min\Delta\phi(E_{\mathrm{T}}^{\mathrm{miss}}, \mathrm{j})$distribution), a 20% systematic uncertainty is added to the W$\to \tau_{\mathrm{h}\nu}$ background estimate cover the small discrepancy in shape of the $\min\Delta\phi(E_{\mathrm{T}}^{\mathrm{miss}}, \mathrm{j})$variable observed between data and MC. Figure 1 shows the data-MC agreement that is obtained in the $\min\Delta\phi(E_{\mathrm{T}}^{\mathrm{miss}}, \mathrm{j})$ variable in each of the control regions.

The QCD multijet process is modelled using the sample of events where the isolation requirement on the $E_{\mathrm{T}}^{\mathrm{miss}}$ has been reversed by requiring that $\min\Delta\phi(E_{\mathrm{T}}^{\mathrm{miss}}, \mathrm{j})$<1.0 but still requiring that the minimum azimuthal angle separation between the leading two jets and the $E_{\mathrm{T}}^{\mathrm{miss}}$, $\min\Delta\phi(E_{\mathrm{T}}^{\mathrm{miss}}, \mathrm{j1/j2})$, be greater than 2.3. These events are normalised in a sideband region to the signal region, which is dominated by QCD. The region chosen is that with $3 < \frac{E_{\mathrm{T}}^{\mathrm{miss}}}{\sigma(E_{\mathrm{T}}^{\mathrm{miss}})} < 4$ and $1.0 < \min\Delta\phi(E_{\mathrm{T}}^{\mathrm{miss}}, \mathrm{j1/j2}) < 2.0$. It is observed that the normalisation factor decreases rapidly as the requirement on $\frac{E_{\mathrm{T}}^{\mathrm{miss}}}{\sigma(E_{\mathrm{T}}^{\mathrm{miss}})}$and $\min\Delta\phi(E_{\mathrm{T}}^{\mathrm{miss}}, \mathrm{j})$are tightened. To model this behaviour the normalisation factor is measured both as a function of the requirement placed on $\frac{E_{\mathrm{T}}^{\mathrm{miss}}}{\sigma(E_{\mathrm{T}}^{\mathrm{miss}})}$and as a function of the requirement placed on $\min\Delta\phi(E_{\mathrm{T}}^{\mathrm{miss}}, \mathrm{j})$. Both functional forms are then extrapolated to the signal region requirements, and as the two variables are correlated the final normalisation factor is taken to be the centre of the envelope formed by the two values obtained.

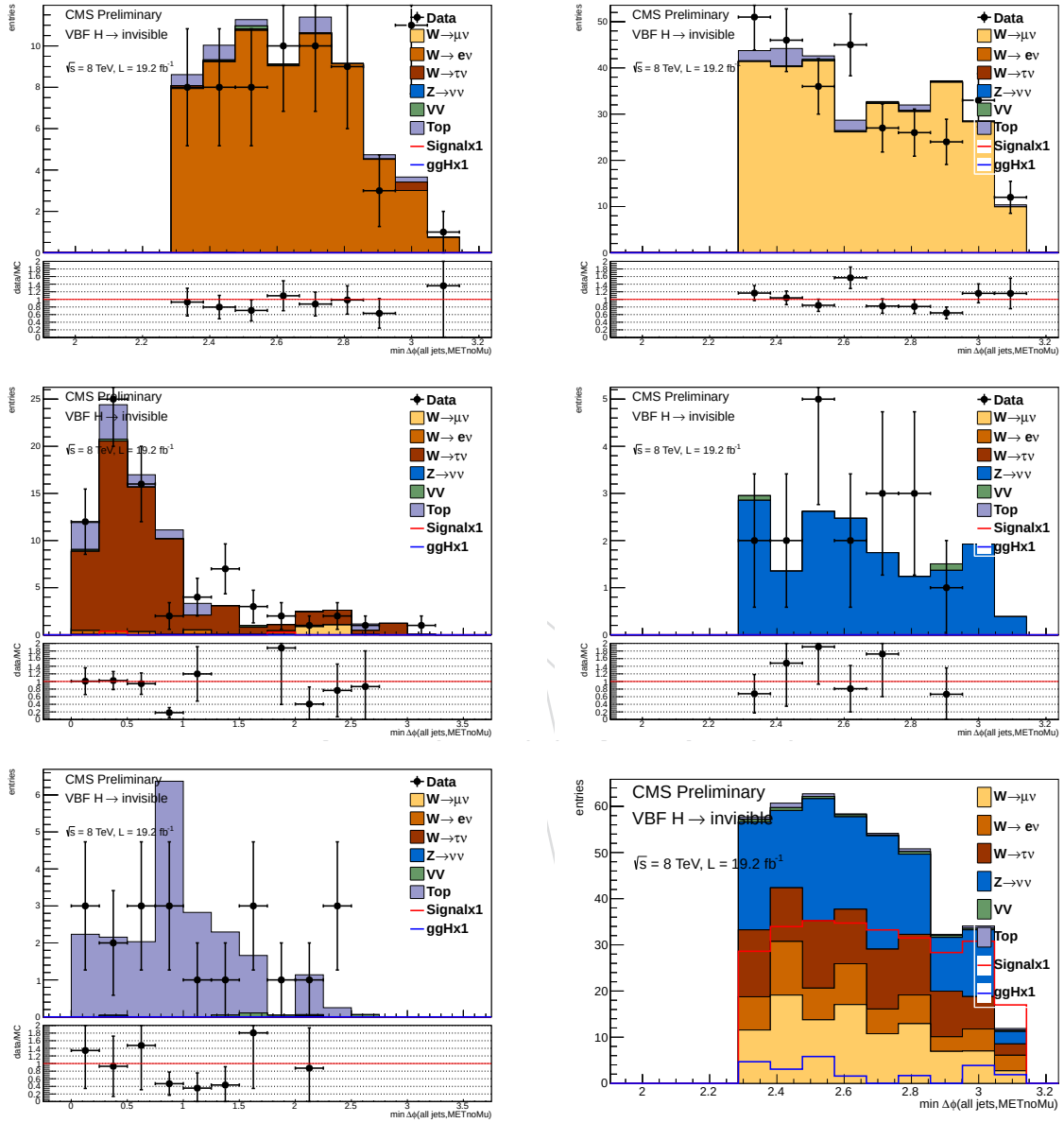

Figure 1: Distribution of the min$\Delta\phi(E_{\mathrm{T}}^{\mathrm{miss}}, \mathrm{j})$ variable in the data and MC, after reweighting the MC to match the data in normalisation. Top row, from left to right: W$\rightarrow e, \mu$ control regions. Middle row from left to right: W$\rightarrow \tau_{\mathrm{h}}$, Z$\rightarrow \mu\mu$ control regions. Bottom row from left to right: top control region, signal region. All plots have the W, Z and top backgrounds normalised to the date in their respective control regions

!

The final number of events for each process that passes the selection is estimated using the MC in the case of the W, Z and top background processes, or the non-isolated $E_{\mathrm{T}}^{\mathrm{miss}}$ events for the QCD multijets process, with the normalisation obtained from the control regions, and is summarised in Table 1. The distribution of the $\min\Delta\phi(E_{\mathrm{T}}^{\mathrm{miss}},\mathrm{j})$ variable in the signal region, with all backgrounds taking their final normalisation is shown in Figure 1. An overview of all considered systematic uncertainties is given in Table 2, with the effect on the sum of all the background processes and the signal with $m_{\mathrm{H}} = 125\,\mathrm{GeV}$ and $\mathcal{B}(\mathrm{H} \to \mathrm{inv}) = 100\%$ given separately.

Table 1: Summary of the estimated number of background and signal events, together with the observed yield, in the VBF search signal region. The signal yield is given for $m_{\mathrm{H}} = 125\,\mathrm{GeV}$ and $\mathcal{B}(\mathrm{H} \to \mathrm{inv}) = 100\%$. The errors quoted are the statistical and systematic uncertainties respectively

Process	Event yields
$Z \to \nu\nu$	$157.3 \pm 37.6 \pm 38.3$
$W \to \mu\nu$	$101.8 \pm 6.1 \pm 11.9$
$W \to e\nu$	$57.4 \pm 7.3 \pm 7.0$
$W \to \tau\nu$	$98.0 \pm 13.2 \pm 25.4$
top	$4.4 \pm 1.0 \pm 1.4$
VV	$3.8 \pm 0.0 \pm 0.7$
QCD multijet	$17 \pm 0 \pm 14$
Total Background	$439.7 \pm 41.0 \pm 55.8$
Signal(VBF)	$273.4 \pm 0.0 \pm 31.2$
Signal(ggH)	$22.6 \pm 0.0 \pm 15.6$

Table 2: Summary of the uncertainties on the total background and signal yields. All uncertainties affect the normalization of the yield, and are quoted as the change in % in the total background or signal estimate, when each systematic effect is varied according to its uncertainties. The signal uncertainties are given for $m_{\mathrm{H}} = 125\,\mathrm{GeV}$ and $\mathcal{B}(\mathrm{H} \to \mathrm{inv}) = 100\%$.

Source	Total background	Signal
Luminosity	0.02	2.60
Lepton ID efficiency	3.22	0.00
Jet energy scale	4.94	10.70
Jet energy resolution	2.86	1.81
Unclustered energy scale	2.28	1.64
Pileup weight	0.95	1.56
MC stat.	5.54	3.82
Control region data stat.	9.30	0.00
$W \to \tau\nu$ control region extrapolation	4.46	0.00
$Z/\gamma^* \to \mu\mu$ to $Z \to \nu\nu$ extrapolation	7.16	0.00
QCD normalisation	3.18	0.00
Theory Uncertainty	0.01	5.14

The dominant uncertainties come from the statistical uncertainty on the number of data events in each of the control regions. In order to estimate the effect of the jet energy scale, unclustered energy scale and jet energy resolution on both the signal and background processes, each quantity is varied separately by its uncertainties in both directions and the full background and signal estimation are repeated. Similarly, the pileup and lepton efficiency scale factors applied to the MC are varied by their uncertainties in both directions. The luminosity uncertainty of

2.6% and the trigger efficiency uncertainty are applied only to the signal and to the minor backgrounds estimated purely from MC. The data-driven normalisation for the main backgrounds ensures that the trigger plateau is properly taken into account. The uncertainties on the diboson cross sections are taken from the CMS published cross-section measurements [28].

Further uncertainties come from the theoretical uncertainty on the cross-section ratio used to extrapolate from QCD produced $Z/\gamma^* \to \mu\mu$ to $Z \to \nu\nu$ in the $Z \to \nu\nu$ background estimation. This uncertainty is estimated by calculating the ratio of yields obtained from both MCFM and MadGraph in a VBF dominated region for both processes. The MCFM NLO result is found to be 1.14, while MadGraph gives 1.2 ± 0.2 resulting in a 20% uncertainty on the $Z \to \nu\nu$ estimate to account for this difference. Theoretical uncertainties on the signal cross-sections due to PDF and QCD scales are taken from the LHC Higgs Cross Section Working Groups Yellow Report 3 [16, 17].

Upper limits on the Higgs boson production cross section times $\mathcal{B}(\mathrm{H} \to \mathrm{inv})$are placed at 95% C.L. using an asymptotic CLs method[29–31], following the standard CMS Higgs combination technique [32, 33]. Systematics uncertainties are treated as nuisance parameters in a frequentist paradigm as described in Ref. [33], and all correlations between processes are taken into account.

Using this procedure and assuming SM Higgs boson production cross-sections and acceptances, the observed (median expected) 95% C.L. limit on $\mathcal{B}(\mathrm{H} \to \mathrm{inv})$of a SM 125 GeV Higgs boson is XX (38)%. The 95% C.L. limit on $\mathcal{B}(\mathrm{H} \to \mathrm{inv})$and the 95% C.L. limit on the cross-section times $\mathcal{B}(\mathrm{H} \to \mathrm{inv})$, both assuming SM Higgs boson acceptances are shown as a function of Higgs boson mass in figure 2.

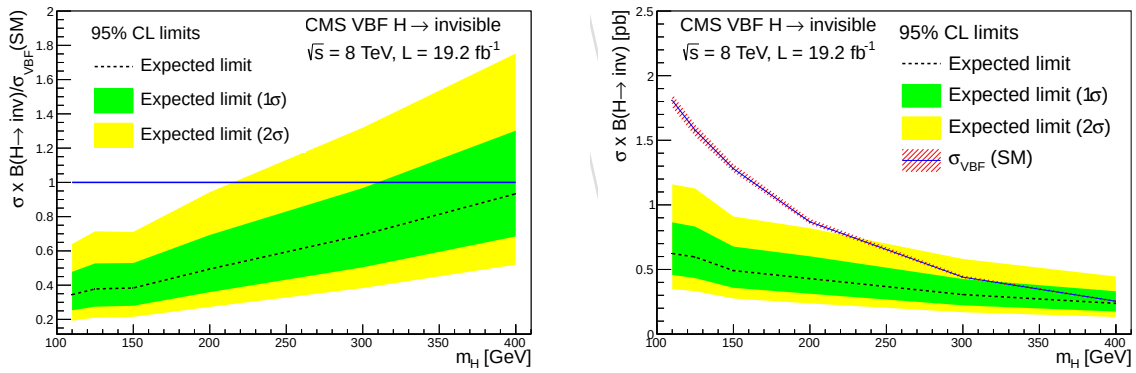

Figure 2: The 95% C.L. limit on $\mathcal{B}(\mathrm{H} \to \mathrm{inv})$of a SM Higgs boson (left) and the 95% C.L. limit on the cross-section times $\mathcal{B}(\mathrm{H} \to \mathrm{inv})$(right)as a function of the Higgs boson mass, assuming SM Higgs boson acceptances.

A search for VBF produced Higgs bosons decaying to invisible final states has been performed. The analysis' sensitivity is increased significantly by the use of triggers recorded as part of the parked data stream. These triggers allow the use a selection driven by enhancing the contribution from $E_{\mathrm{T}}^{\mathrm{miss}}$ coming from genuine invisible particles isolated from jet activity in the transverse plane, rather than mismeasured energy or $E_{\mathrm{T}}^{\mathrm{miss}}$ from heavy-flavoured jet decays. The observed (median expected) limit on $\mathcal{B}(\mathrm{H} \to \mathrm{inv})$of a SM Higgs with $m_{\mathrm{H}} = 125\,\mathrm{GeV}$ is XX (38)%.

Acknowledgements

We congratulate our colleagues in the CERN accelerator departments for the excellent performance of the LHC and thank the technical and administrative staffs at CERN and at other CMS institutes for their contributions to the success of the CMS effort. In addition, we gratefully acknowledge the computing centres and personnel of the Worldwide LHC Computing Grid for delivering so effectively the computing infrastructure essential to our analyses. Finally, we acknowledge the enduring support for the construction and operation of the LHC and the CMS detector provided by the following funding agencies: BMWFW and FWF (Austria); FNRS and FWO (Belgium); CNPq, CAPES, FAPERJ, and FAPESP (Brazil); MES (Bulgaria); CERN; CAS, MoST, and NSFC (China); COLCIENCIAS (Colombia); MSES and CSF (Croatia); RPF (Cyprus); MoER, ERC IUT and ERDF (Estonia); Academy of Finland, MEC, and HIP (Finland); CEA and CNRS/IN2P3 (France); BMBF, DFG, and HGF (Germany); GSRT (Greece); OTKA and NIH (Hungary); DAE and DST (India); IPM (Iran); SFI (Ireland); INFN (Italy); MSIP and NRF (Republic of Korea); LAS (Lithuania); MOE and UM (Malaysia); CINVESTAV, CONACYT, SEP, and UASLP-FAI (Mexico); MBIE (New Zealand); PAEC (Pakistan); MSHE and NSC (Poland); FCT (Portugal); JINR (Dubna); MON, RosAtom, RAS and RFBR (Russia); MESTD (Serbia); SEIDI and CPAN (Spain); Swiss Funding Agencies (Switzerland); MST (Taipei); ThEPCenter, IPST, STAR and NSTDA (Thailand); TUBITAK and TAEK (Turkey); NASU and SFFR (Ukraine); STFC (United Kingdom); DOE and NSF (USA).

References

[1] ALEPH, DELPHI, L3, and OPAL Collaborations, LEP Higgs Working Group, "Searches for invisible Higgs bosons: Preliminary combined results using LEP data collected at energies up to 209-GeV", (2001). arXiv:hep-ex/0107032.

[2] DELPHI Collaboration, "Searches for invisibly decaying Higgs bosons with the DELPHI detector at LEP", *Eur. Phys. J. C* **32** (2004) 475, doi:10.1140/epjc/s2003-01469-8, arXiv:hep-ex/0401022.

[3] OPAL Collaboration, "Search for invisibly decaying Higgs bosons with large decay width using the OPAL detector at LEP", *Eur. Phys. J. C* **49** (2007) 457, doi:10.1140/epjc/s10052-006-0170-x, arXiv:hep-ex/0610056.

[4] ATLAS Collaboration, "Search for Invisible Decays of a Higgs Boson Produced in Association with a Z Boson in ATLAS", *Phys. Rev. Lett.* **112** (2014) 201802, doi:10.1103/PhysRevLett.112.201802, arXiv:1402.3244.

[5] ATLAS Collaboration, "Search for dark matter in events with a hadronically decaying W or Z boson and missing transverse momentum in pp collisions at $\sqrt{s} = 8$ TeV with the ATLAS detector", *Phys. Rev. Lett.* **112** (2014) 041802, doi:10.1103/PhysRevLett.112.041802, arXiv:1309.4017.

[6] CMS Collaboration Collaboration, "Search for invisible decays of Higgs bosons in the vector boson fusion and associated ZH production modes", *Eur.Phys.J.* **C74** (2014), no. 8, 2980, doi:10.1140/epjc/s10052-014-2980-6, arXiv:1404.1344.

[7] CMS Collaboration, "CMS Luminosity Based on Pixel Cluster Counting – Summer 2013 Update", CMS Physics Analysis Summary CMS-PAS-LUM-13-001, 2013.

[8] CMS Collaboration, "The CMS experiment at the CERN LHC", *JINST* **3** (2008) S08004, doi:10.1088/1748-0221/3/08/S08004.

[9] P. Nason, "A new method for combining NLO QCD with shower Monte Carlo algorithms", *JHEP* **11** (2004) 040, doi:10.1088/1126-6708/2004/11/040, arXiv:hep-ph/0409146.

[10] S. Frixione, P. Nason, and C. Oleari, "Matching NLO QCD computations with parton shower simulations: the POWHEG method", *JHEP* **11** (2007) 070, doi:10.1088/1126-6708/2007/11/070, arXiv:0709.2092.

[11] S. Alioli, P. Nason, C. Oleari, and E. Re, "NLO single-top production matched with shower in POWHEG: s- and t-channel contributions", *JHEP* **09** (2009) 111, doi:10.1088/1126-6708/2009/09/111, arXiv:0907.4076. [Erratum: doi:10.1007/JHEP02(2010)011].

[12] K. Hamilton, P. Richardson, and J. Tully, "A positive-weight Next-to-Leading Order Monte Carlo simulation for Higgs boson production", *JHEP* **09** (2009) 116, doi:10.1088/1126-6708/2009/04/116, arXiv:0903.4345.

[13] P. Nason and C. Oleari, "NLO Higgs boson production via vector-boson fusion matched with shower in POWHEG", *JHEP* **02** (2010) 037, doi:10.1007/JHEP02(2010)037, arXiv:0911.5299.

[14] S. Alioli, P. Nason, C. Oleari, and E. Re, "A general framework for implementing NLO calculations in shower Monte Carlo programs: the POWHEG BOX", *JHEP* **06** (2010) 043, doi:10.1007/JHEP06(2010)043, arXiv:1002.2581.

[15] E. Re, "Single-top Wt-channel production matched with parton showers using the POWHEG method", *Eur. Phys. J. C* **71** (2011) 1547, doi:10.1140/epjc/s10052-011-1547-z, arXiv:1009.2450.

[16] LHC Higgs Cross Section Working Group, S. Dittmaier et al., "Handbook of LHC Higgs Cross Sections: 1. Inclusive Observables", CERN Report CERN-2011-002, 2011. doi:10.5170/CERN-2011-002, arXiv:1101.0593.

[17] LHC Higgs Cross Section Working Group, S. Dittmaier et al., "Handbook of LHC Higgs Cross Sections: 2. Differential Distributions", CERN Report CERN-2012-002, 2012. doi:10.5170/CERN-2012-002, arXiv:1201.3084.

[18] J. Alwall et al., "MadGraph 5: going beyond", *JHEP* **06** (2011) 128, doi:10.1007/JHEP06(2011)128, arXiv:1106.0522.

[19] T. Sjöstrand, S. Mrenna, and P. Z. Skands, "PYTHIA 6.4 physics and manual", *JHEP* **05** (2006) 026, doi:10.1088/1126-6708/2006/05/026, arXiv:hep-ph/0603175.

[20] GEANT4 Collaboration, "GEANT4—a simulation toolkit", *Nucl. Instrum. Meth. A* **506** (2003) 250, doi:10.1016/S0168-9002(03)01368-8.

[21] CMS Collaboration, "Particle–Flow Event Reconstruction in CMS and Performance for Jets, Taus, and $E_{\mathrm{T}}^{\mathrm{miss}}$", CMS Physics Analysis Summary CMS-PAS-PFT-09-001, 2009.

[22] CMS Collaboration, "Commissioning of the particle-flow event reconstruction with the first LHC collisions recorded in the CMS detector", CMS Physics Analysis Summary CMS-PAS-PFT-10-001, 2010.

[23] CMS Collaboration, "Performance of tau-lepton reconstruction and identification in CMS", *JINST* **7** (2012) P01001, doi:10.1088/1748-0221/7/01/P01001, arXiv:1109.6034.

[24] M. Cacciari, G. P. Salam, and G. Soyez, "The anti-k_t jet clustering algorithm", *JHEP* **04** (2008) 63, doi:10.1088/1126-6708/2008/04/063, arXiv:0802.1189.

[25] M. Cacciari, G. P. Salam, and G. Soyez, "FastJet user manual", *Eur. Phys. J. C* **72** (2012) 1896, doi:10.1140/epjc/s10052-012-1896-2, arXiv:1111.6097.

[26] M. Cacciari and G. P. Salam, "Dispelling the N^3 myth for the k_t jet-finder", *Phys. Lett. B* **641** (2006) 57, doi:10.1016/j.physletb.2006.08.037, arXiv:hep-ph/0512210.

[27] CMS Collaboration, "Determination of jet energy calibration and transverse momentum resolution in CMS", *JINST* **6** (2011) P11002, doi:10.1088/1748-0221/6/11/P11002, arXiv:1107.4277.

[28] CMS Collaboration, "Measurement of W^+W^- and ZZ production cross sections in pp collisions at $\sqrt{s} = 8$ TeV", *Phys. Lett. B* **721** (2013) 190, doi:10.1016/j.physletb.2013.03.027, arXiv:1301.4698.

[29] A. L. Read, "Presentation of search results: the CL_s technique", *J. Phys. G* **28** (2002) 2693, doi:10.1088/0954-3899/28/10/313.

[30] T. Junk, "Confidence level computation for combining searches with small statistics", *Nucl. Instrum. Meth. A* **434** (1999) 435, doi:10.1016/S0168-9002(99)00498-2.

[31] LHC Higgs Cross Section Working Group, S. Dittmaier, C. Mariotti, G. Passarino, R. Tanaka (Eds.), "Handbook of LHC Higgs Cross Sections: Differential Distributions", CERN Report CERN-2012-002, 2012. arXiv:1201.3084.

[32] CMS Collaboration, "Observation of a new boson with mass near 125 GeV in pp collisions at $\sqrt{s} = 7$ and 8 TeV", *JHEP* **06** (2013) 081, doi:10.1007/JHEP06(2013)081, arXiv:1303.4571.

[33] ATLAS and CMS Collaborations, LHC Higgs Combination Group, "Procedure for the LHC Higgs boson search combination in Summer 2011", Technical Report ATL-PHYS-PUB-2011-11, CMS NOTE 2011/005, 2011.